Scientia Horticulturae 310 (2023) 111714

Contents lists available at ScienceDirect

Scientia Horticulturae

journal homepage: www.elsevier.com/locate/scihorti

Modeling mango ripening during shelf life based on pulp color nondestructively measured by time-resolved reflectance spectroscopy

Maristella Vanoli [a,*], Anna Rizzolo [a], Maurizio Grassi [a], Lorenzo Spinelli [b], Alessandro Torricelli [b,c]

[a] Consiglio per la ricerca in agricoltura e l'analisi dell'economia agraria (CREA), Centro di Ricerca Ingegneria e Trasformazioni agroalimentari (CREA-IT), via Venezian 26, 20133 Milano, Italy
[b] Istituto di Fotonica e Nanotecnologie, Consiglio Nazionale delle Ricerche (IFN-CNR), Piazza L. da Vinci 32, 20133 Milano, Italy
[c] Politecnico di Milano, Dipartimento di Fisica, Piazza L. da Vinci 32, 20133 Milano, Italy

ARTICLE INFO

Keywords:
Mangifera indica L.
Shelf life
Biological shift factor
μ_a540 modeling
Pulp color kinetic models

ABSTRACT

Non-destructive techniques could help mango growers to pick fruit at the proper maturity degree and to monitor fruit quality during storage and marketing to satisfy the consumer expectations. The absorption coefficient non-destructively measured at 540 nm (μ_a540) by time-resolved reflectance spectroscopy (TRS) was shown to be a maturity index for mango fruit and was highly correlated with pulp color parameters and carotenoids content. The aim of this work was to model μ_a540 using the biological shift factor theory to verify if μ_a540 is able to assess the maturity degree of individual mango fruit and then to use μ_a540 to model pulp color in order to relate μ_a540 to an important index of mango ripening.

Mango fruit (*Mangifera indica* L. cv Tommy Atkins) at commercial maturity for ship and air transport maturities, were measured by TRS, ranked according to decreasing μ_a540 (decreasing maturity), randomized into six batches per transport maturity and analyzed for μ_a540 and pulp color parameters after 0, 1, 2, 5, 6 and 7 days of shelf life at 20 °C.

The μ_a540 as a function of biological shift factor increased during ripening following a logistic/exponential model (R^2_{adj}=99%) with a faster rate in less mature fruit than in more mature ones. The changes in pulp color during mango ripening depended on fruit maturity (i.e., μ_a540) and on time of shelf life at 20 °C. By converting the μ_a540 into the biological shift factor it was possible to model the increasing trend of a^*, b^*, C^*, and I_Y and the decreasing trend of L^* and h° during the shelf life period explaining 91.2–99.8% of the variation and to differentiate mango fruit according to their biological age. Similarly to μ_a540, color changes occurred earlier in more mature fruit and later in less mature ones with the same pattern in time.

There is a synchronization between changes of μ_a540 and changes of a^*, b^*, C^* and yellowness during ripening in mango fruit which allows to use μa540 to sort fruit according to their maturity degree and then to optimize fruit management along the supply chain.

1. Introduction

Mango (*Mangifera indica* L.) is a tropical/subtropical climacteric fruit that is typically harvested at hard green stage, providing time for transport to distant markets and marketing.

Firmness, pulp color, total soluble solids content, dry matter, titratable acidity and aroma volatiles are the main attributes related to ripening in mango fruit. Flesh color is an important indicator of maturity and ripeness as all mango cultivars develop yellow and orange pigments due to carotenoids accumulation in the flesh during maturity and ripening, while changes in skin color are not always correlated with maturity, ripeness or internal eating quality (Padda et al., 2011). During ripening, mesocarp tissue color changes exhibiting a progressive decrease in L* and h° values while flesh a*, b* and C* values increased (Padda et al., 2011). The best color attributes to follow changes during mango ripening are a* and b* of the flesh with b* showing the highest

* Corresponding author at: Consiglio per la ricerca in agricoltura e l'analisi dell'economia agraria (CREA), Centro di Ricerca Ingegneria e Trasformazioni agroalimentari (CREA-IT), via Venezian 26, I-20133 Milano, Italy.
E-mail address: maristella.vanoli@crea.gov.it (M. Vanoli).

https://doi.org/10.1016/j.scienta.2022.111714
Received 3 March 2022; Received in revised form 16 November 2022; Accepted 17 November 2022
Available online 7 December 2022

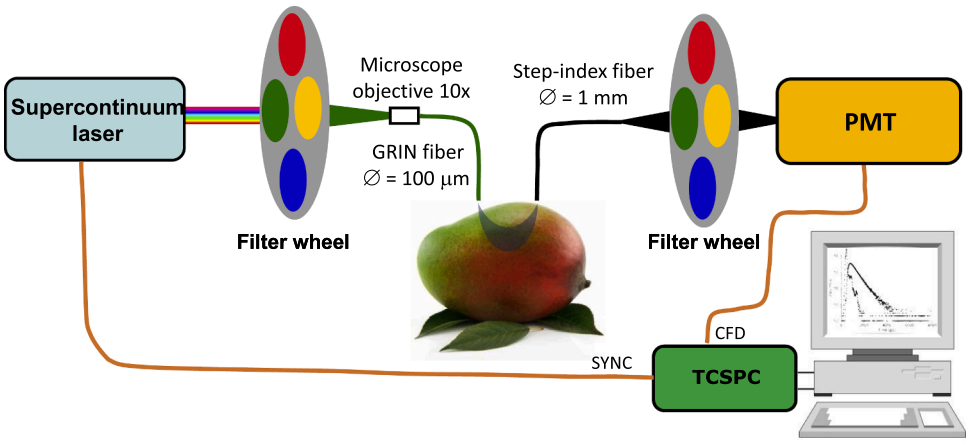

Fig. 1. Scheme of the setup used for TRS measurements on mango fruit. GRIN: graded-index; PMT: photomultiplier tube; SYNC: synchronization signal; CFD: constant fraction discriminator signal; TCSPC: time-correlated single-photon counting board.

correlation with maturity score and dry matter (Subedi et al., 2007; Kienzle et al., 2011; Padda et al., 2011).Unfortunately, mesocarp color can be measured only in a destructive way; therefore, the development of non-destructive techniques could help growers to pick fruit at the proper maturity degree for each market destination (local, distant) especially in the view of minimizing quantitative and qualitative losses during the supply chain. Among optical methods, continuous wave near infrared (NIR) or visible (Vis) -NIR spectroscopy has been used for predicting pulp color (Subedi et al., 2007; Cortés et al., 2016). This approach, however, predicts maturity parameters indirectly and the robustness of the prediction model is linked to the extent and variation of the population used for the calibration. An improvement with respect to the standard Vis-NIR approach could be the direct non-destructive measure of the relevant parameters in the fruit mesocarp, which can be achieved by the time-resolved reflectance spectroscopy (TRS) or space- resolved reflectance spectroscopy (SRS) techniques.

TRS and SRS, differently from continuous wave methods, can simultaneously measure the effects of light absorption, due to chemical compounds, and of light scattering, mainly due to microscopic changes in refractive index caused by membranes, organelles, vacuoles, starch granules and air (Lu et al., 2020). In TRS, a short pulse of monochromatic light is injected into the fruit: whenever a photon strikes a scattering center, it changes its trajectory and keeps on propagating in the tissue, until it is eventually reemitted across the boundary, or it is captured by an absorbing center. Usually, the laser light is injected into and collected from the fruit by using two optical fibres placed in contact with the surface at a distance of 1–2 cm. The laser light probes a banana-shaped volume of tissue to a depth of 1–2 cm, in contrast to continuous-wave Vis-NIR spectrophotometers, which have a useful penetration depth of a few millimeters, depending on the wavelength (Lammertyn et al., 2000). By measuring the photon distribution of time-of-flight both the absorption (μ_a) and reduced scattering (μ_s') coefficients in the Vis–NIR spectrum region are estimated (Cubeddu et al., 2001; Torricelli et al., 2008). TRS relies on the ability to measure the optical properties of the fruit mesocarp with no or limited influence from the skin as the spectra acquired on whole fruit for both absorption and scattering were shown to be very similar to the spectra of the same fruit when peeled (Cubeddu et al., 2001; Saeys et al., 2008; Torricelli et al., 2008; Spinelli et al., 2012; Rizzolo and Vanoli, 2016).

TRS has been used to study the internal fruit attributes related to maturity (Rizzolo and Vanoli, 2016). The μ_a measured in the chlorophyll-*a* absorption region near 670 nm is considered an index of the biological age of the fruit and have been used to define harvest maturity and to model fruit ripening on an individual fruit basis. Fruit maturity on the tree is not homogeneous but depends on flowering time, position of fruit on the tree relative to leaves and other fruit, microclimate and hormonal and nutritional effects. This variability can be expressed as biological shift factor (BSF, Tijskens et al., 2005). In nectarines (Tijskens et al., 2007b) and in apples (Rizzolo et al., 2021), μ_a670 declines during fruit ripening and was successfully used to predict the softening rate in nectarines and to select fruit for different market destinations (Eccher Zerbini et al., 2009; Rizzolo et al., 2021) when it was converted into the biological shift factor In mangoes, Pereira et al. (2010) showed that μ_a630 could be used to predict softening rate of 'Tommy Atkins' mangoes, even if the model explained only 70% of the variation in firmness decay, whereas Eccher Zerbini et al. (2015) by using both μ_a670 and μ_a540 (carotenoid tail) in 'Haden' mangoes was able to assess fruit maturity and to predict the ripening of individual fruit with 80% of variability explained for the ethylene and firmness logistic models. Rizzolo et al. (2016) and Vanoli et al. (2018) reported that μ_a540 can be used as a non-destructive maturity index for mangoes, as it was able to classify intact mangoes of different cultivars according to pulp color and to the contents of total and individual carotenoids.

However, until now no model was developed combining μ_a540 and the BSF for assessing ripening in mangoes, as achieved for μ_a670 in nectarines and in apples. Hence, the aim of this work was to model μa540 using the biological shift factor theory to verify if μa540 is able to assess the maturity degree of individual mango fruit and then to use μa540 to model pulp color in order to relate μa540 to an important index of mango ripening.

2. Materials and methods

2.1. TRS instrumentation

A scheme of the portable TRS setup developed at Politecnico di Milano and used for measurements is reported in Fig. 1. It is based on a supercontinuum fiber laser (SC450–6 W, Fianium, UK) as a source, that provides white-light picosecond pulses, adjustable in power by means of a variable neutral-density attenuator. The spectral selection of the injected light is performed through a filter wheel loaded with 14 band-pass interference filters with characteristic wavelengths in the range 540 - 940 nm. Light is, then, delivered to the sample exploiting a 100 µm-diameter multimode graded-index fiber.

As for the detection side, diffuse re-emitted light by the sample is collected by a 1 mm-diameter step-index fiber 1.5 cm apart from the injection point, and delivered to a photomultiplier (HPM-100–50, Becker&Hickl, Germany) for detection. Finally, by means of a time-correlated single-photon counting board (SPC-130, Becker&Hickl, Germany), distributions of time-of-flight of re-emitted photons at different wavelengths are recorded. Further details of this instrumentation can be found in Spinelli et al. (2012).

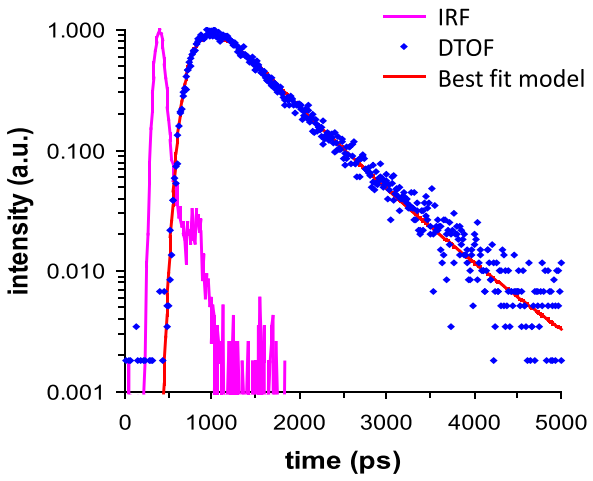

Fig. 2. Exemplum of the best fit of the model (red line), describing photon diffusion in a turbid medium, on measured DTOF (blue dots) after convolution with instrument IRF (pink line). (For interpretation of the references to colour in this figure legend, the reader is referred to the web version of this article.)

In order to assess the optical properties of the sample, recorded DTOFs (distribution of photon time-of-flight) have been analyzed with a model describing the photon diffusion in turbid media based on the solution of the diffusion equation in a homogeneous semi-infinite medium (Martelli et al., 2009). In particular, after a convolution with the instrument response function (IRF), the model was best fitted to the recorded DTOF considering the absorption and reduced scattering coefficients as free parameters. This analysis procedure is depicted in Fig. 2.

2.2. Fruit

Mango fruit (*Mangifera indica* L., cv 'Tommy Atkins') were harvested in commercial orchards in Pernambuco (Brazil) at commercial maturities for ship- and air- transport, which had been defined according to the importer's protocol for each type of shipping (less mature for ship – longer transport time; more mature for air – shorter transport time), and carried by plane to Milano (Italy) immediately after harvest. According to the diagram shown in Fig. 3, on arrival at CREA-IT lab (about 5–7 days from harvest), 180 fruits per type of transport were selected, measured by TRS at 540 nm on two opposite sides in the fruit equatorial region and ranked within each type of transport by decreasing μ_a540 averaged over the two sides, that is from more (high μ_a) to less mature fruit (low μ_a). The ranked fruit were grouped by 6, for a total of 30 groups, corresponding to 30 levels of μ_a540. Each fruit from each group was randomly assigned to a different sample. In this way, 6 samples per type of shipping were obtained, each one containing 30 fruits from the whole range of μ_a540 and used for a single time of shelf life at 20 °C: 0, 1, 2, 5, 6, and 7 days (labelled d0, d1, d2, d5, d6 and d7, respectively).

Then at each shelf-life time, μ_a540 and pulp color was measured in correspondence of the positions of TRS measurements with a spectrophotometer (CM-2600d, Minolta Co., Japan), using the primary illuminant D65 and 2° observer in the L^*, a^*, b^* color space. From the L^*, a^* and b^* values, hue (h°), chroma (C^*) and Yellowness Index (I_Y) were computed according to the following equations:

$$h^\circ = \arctan(b^*/a^*) \times 360/(2 \times 3.14) \quad (1)$$

$$C* = \left(a^{*2} + b^{*2}\right)^{-2} \quad (2)$$

$$I_Y = [(81.2746X - - 1.0574Z)/Y] \times 100 \quad (3)$$

after converting $L^*a^*b^*$ parameters into the XYZ color space (Jha et al., 2006). Data were averaged per fruit.

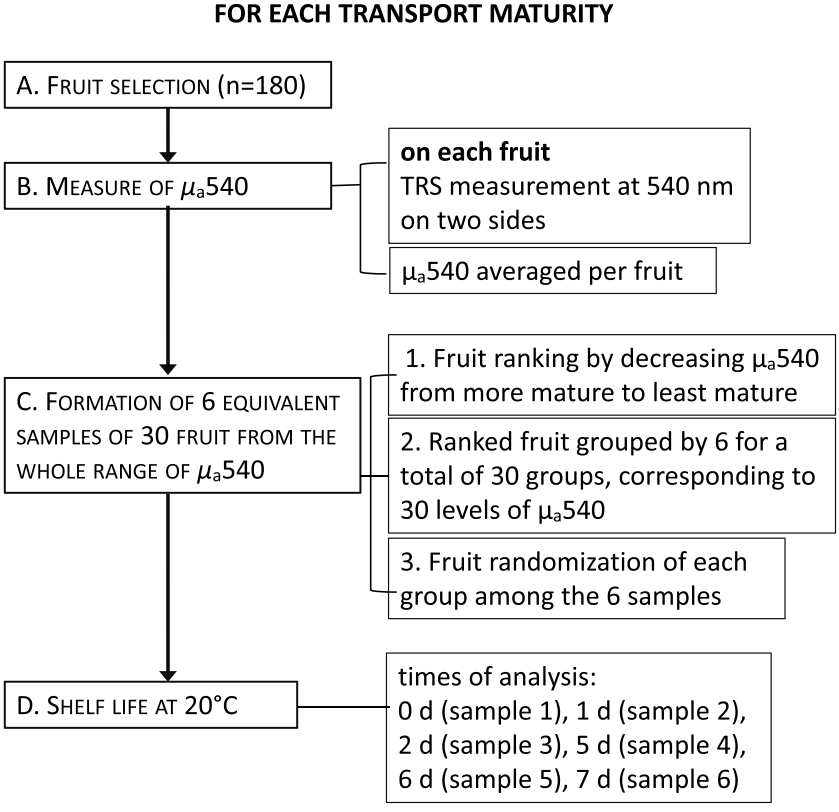

Fig. 3. Diagram of the procedure used for the formation of the six equivalent samples of 30 fruit.

The sample d7 was measured by TRS at 540 nm also at times 0, 1, 2, 5 and 6 days of shelf-life.

2.3. The $\mu_a 540$ model

Basing on the fact that several biological phenomena such as color development, fruit softening and chlorophyll degradation, develop or decay following a sigmoid curve, in order to model the μ_a540 behavior with the fruit biological age, it was assumed that the increase of μ_a540, mainly due to carotenoids development, follows a sigmoid curve increasing with the biological age of the fruit, which can be described using the logistic model (Penchaiya et al., 2020) of Eq. (4):

$$y = \left(y_{ref} - y_{min}\right) \times e^{-km\times(t+\Delta t)} + y_{min} \quad (4)$$

where: y is μ_a540; t is the time of shelf life; km is the rate constant and Δt the biological shift factor. The y_{min} is the minimum μ_a540 value ever possible at minus infinite time, y_{ref} is the chosen reference value of μ_a540 at which the BSF equals zero, i.e., the midpoint of the overall range of change in μ_a540.

The BSF Δt is a stochastic variable containing all the information related to maturity for each individual fruit in the whole batch, and is the shift of individual maturity in relation to the intermediate maturity ($\Delta t = 0$) corresponding to μ_a540 equal to half of the maximum and can be computed according to Eq. (5) (Tijskens et al., 2010):

$$\Delta t = -\left(\frac{log\left(\frac{y_0 - y_{min}}{y_{ref} - y_{min}}\right)}{km}\right) \quad (5)$$

where y_0 is the μ_a540 value of the fruit used for fruit ranking at the start of the experiment.

2.4. Color parameters models

It has been shown that color parameters with ripening follows a sigmoidal curve (Penchaiya et al., 2015, 2020). For b^*, C^* and I_Y it was assumed that these y color parameters could follow a sigmoid curve increasing with the biological age of the fruit reaching a maximum value (y_{max}):

$$y = \frac{y_{max}}{1 + e^{\left(-k_m\times\left(t+\Delta t_y^*\right)\right)}} \quad (6)$$

while for a^* the model (7), in which y_{min}, the minimum value ever possible, is included and the range of values replaces y_{max}, best fitted a^* data ranging from negative to positive values:

$$y = y_{min} + \frac{\left(y_{max} - y_{min}\right)}{1 + e^{\left(-k_m\times\left(t+\Delta t_y^*\right)\right)}} \quad (7)$$

As for L^* and h°, it was assumed that these y color parameters decrease with ripening to minimum values without reaching the zero value:

$$y = y_{min} + \frac{y_{max} - y_{min}}{1 + e^{k_m\times\left(t+\Delta t_y^*\right)}} \quad (8)$$

In these models, y_{max} and y_{min} are the maximum and minimum values ever possible for the y color parameter (at minus and plus infinite time), k_m is the rate constant for the color parameter y, t is the normalized time which is zero when the value of the y color parameter is halfway between its maximum and minimum values within each set, and Δt_y^* is the BSF in time relative to time $t = 0$ for the y color parameter, which accounts for the different age of individual fruit in regard to a^*, b^*, C^* and yellowness index increases and L^* and h° decreases.

By these models moreover it was assumed that all fruit, grown in the same orchard and edaphic conditions, had the same behavior as regard to L^*, a^*, b^*, C^*, h° and I_Y while ripening, and each fruit, with its BSF, represents a different step of the same process. As described for μ_a540, Δt_y^* is a stochastic variable containing all the information related to maturity for each individual fruit in the whole batch, expressed in standardized dimensionless time Tjiskens et al., 2007a). Since the increase of a^*, b^*, C^* and I_Y was positively related to the exponential increase of carotenoids during ripening (Ornelas-Paz et al., 2008), and that μ_a540 was positively related to total carotenoids in mango (Vanoli et al., 2016; Vanoli et al., 2018) and negatively related to L^* and h° (Spinelli et al., 2012; Vanoli et al., 2016), it can be assumed that the BSF of each color parameter (Δt_y^* in the Eqs. (6), ((7) and (8)) could be expressed as a function of the measured μ_a540 ($\mu_a 540_0$) relatively to its range

$$\begin{aligned} \Delta t_y^* &= \alpha_{540} \times \delta + \beta \text{ with} \\ \delta &= \log \frac{\mu a 540_{max} - \mu a 540_0}{\mu a 540_0 - \mu a 540_{min}} \end{aligned} \quad (9)$$

where α_{540} and β are parameters to be estimated. The subscript 0 indicates the μ_a540 value measured in each fruit by TRS on the same day as color parameters measurement, while the indices max and min indicate the maximum (0.84 cm^{-1}) and minimum (0.05 cm^{-1}) values ever possible found in experiments on mango fruit, where extreme values were found Eccher Zerbini et al., 2015). To express Δt_y^* in time dimension, in Eqs. (6), ((7) and (8), this variable was divided by the range of the y color parameter and the rate constant k_m.

2.5. Statistics

Modeling of μ_a540 in shelf life was carried out using Statgraphics ver. 5.1 Plus (Manugistic Inc., Rockville, MD, USA). From model (4) combined with Eq. (5), k_m was estimated using the non-linear regression procedure, in which y_{min} was fixed to 0.08 cm^{-1} on the basis of μ_a540 data obtained in this or other experiments with mango fruit, y_{ref} was equal for each data set to the mean of μ_a540 values of all the fruit of the set at the start of the experiment (sorting), y_0 is the μ_a540 value of the fruit used for fruit ranking at the start of the experiment, and t was expressed in days of shelf life. The initial k_m was set at 0.0001 and the estimation was carried out by the Marquardt method and stopped when the convergence of residual sum of squares was achieved. In the non-linear regression procedure y_0 and t were considered independent variables and the fruit μ_a540 value was the dependent variable. The rate constant k_m was estimated considering the μ_a540 value of the 30 fruits of sample d7 during the whole period of shelf-life. Then, both for sample d7 in shelf life and for d0, d1, d2, d5, d6 and d7 samples, the Δt of each individual fruit was computed according to Eq. (4) using the estimated rate constant for the specific data set (ship-transport maturity, air-transport maturity, ship+air set). Then, using the regression analysis procedure, the models of μ_a540 vs. $t+\Delta t$, with t being the normalized time, with 0 value when μ_a540 is in the midpoint between the minimum and the maximum value, were studied.

Color data were analyzed by non-linear regression (Statgraphics ver. 5.1 Plus, Manugistic Inc., Rockville, MD, USA) to be represented as functions of fruit maturity at the time of measure, as assessed by μ_a540 optical property. From model (6) for b^*, C^* and I_Y, model (7) for a^* and model (8) for L^* and h°, all combined with Eq. (9), k_m, α540 and β were estimated, after having computed for each fruit the δ value. Then, Δt_y^* of each individual fruit for every color parameter was computed according to Eq. (9), and expressed in the time dimension by dividing it by the range and k_m. Then, using the regression analysis procedure, the models of each color parameter vs. Δt_y^* expressed in time dimension, were studied.

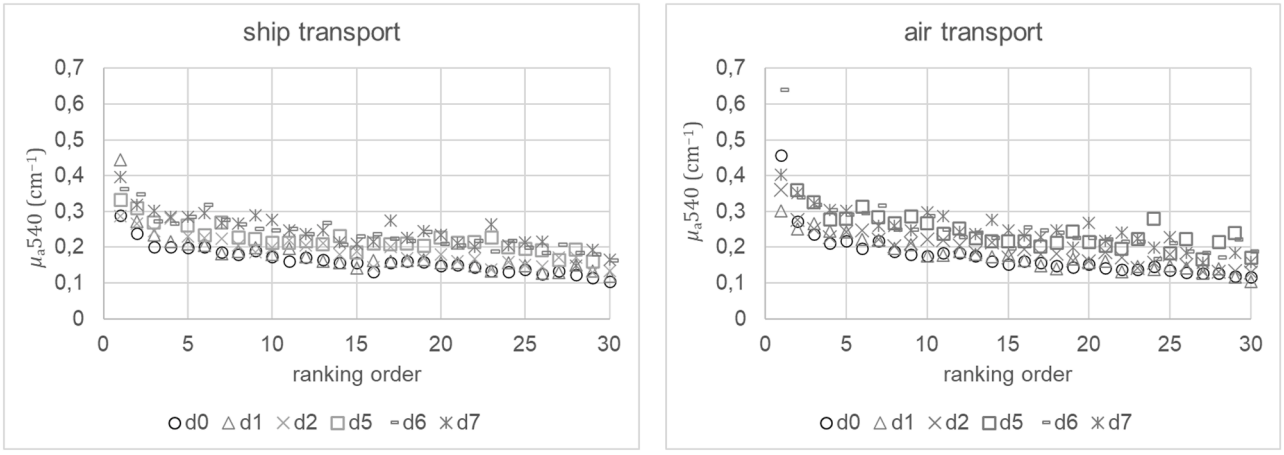

Fig. 4. Absorption coefficient μ_a540 of fruit of d0, d1, d2, d5, d6 and d7 samples of ship (left) and air (right) transport maturity degree at harvest according to ranking order.

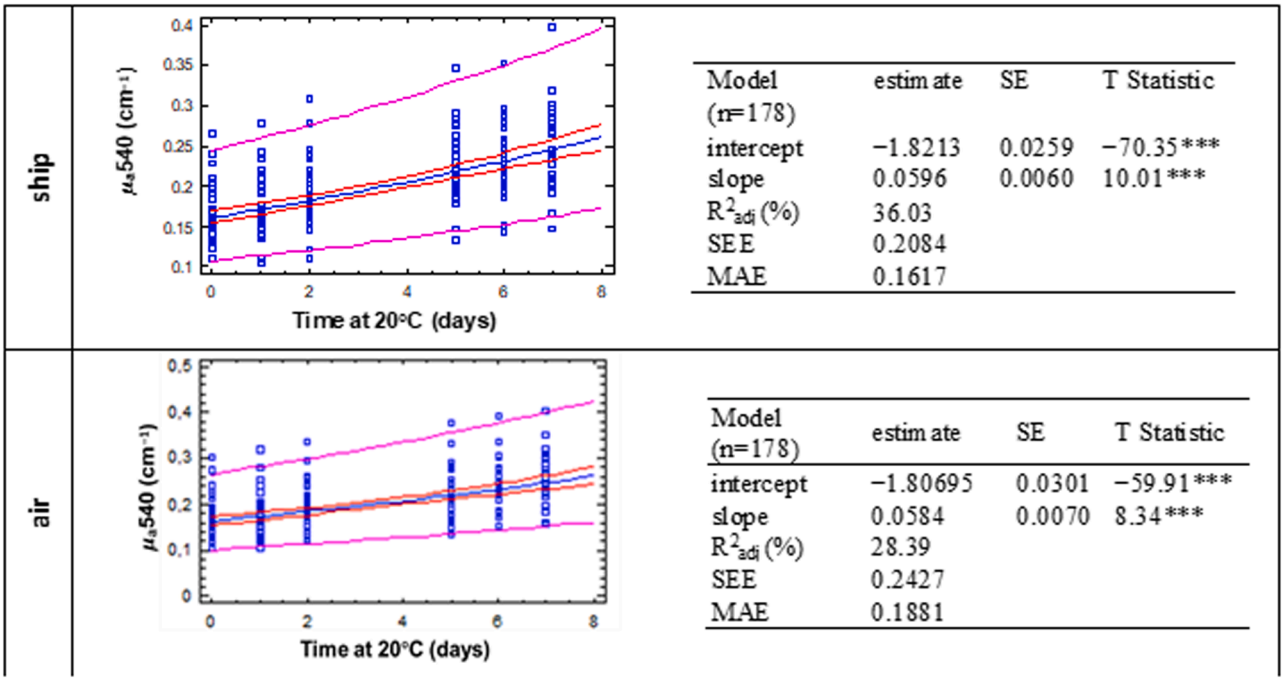

Model (n=178)	estimate	SE	T Statistic
intercept	−1.8213	0.0259	−70.35***
slope	0.0596	0.0060	10.01***
R^2_{adj} (%)	36.03		
SEE	0.2084		
MAE	0.1617		

Model (n=178)	estimate	SE	T Statistic
intercept	−1.80695	0.0301	−59.91***
slope	0.0584	0.0070	8.34***
R^2_{adj} (%)	28.39		
SEE	0.2427		
MAE	0.1881		

Fig. 5. Absorption coefficient at 540 nm (μ_a540) of sample d7 of ship and air transport maturities in function of time of shelf life at 20 °C: fitted exponential model, confidence limits at 95% level (inner lines), prediction limits (outer lines) and experimental data (left) and estimates and standard error (SE) of intercept and slope, R-squared adjusted for d.f. (R^2_{adj}), standard error of the estimate (SEE) and mean absolute error (MAE) of the fitted model (right).

Table 1
Estimates of the rate constant of μ_a540 increase in time (*km*), asymptotic standard error and 95% confidence interval of k_m estimate, R^2_{adj}, standard error of the estimate (SEE) and mean absolute error (MAE) of the Eq. (4) model for ship, air and ship+air transport maturities data sets.

Data set	n	*Km*				model		
		estimate	Asymptotic SE	Asymptotic 95% confidence interval				
				lower	upper	R^2_{adj}	SEE	MAE
ship	177	0.10839	0.00246	0.10353	0.11325	82.6	0.0272	0.0180
air	177	0.09356	0.00316	0.08733	0.09979	77.7	0.0321	0.0220
Ship+air	354	0.09991	0.00206	0.09587	0.100396	79.0	0.0285	0.0202

Table 2
BSF for μ_a540 ($\Delta t_{\mu a540}$) of sample d7 of ship and air data sets during shelf life at 20 °C: minimum, maximum, mean, standard deviation values of distributions and results of tests for normality ($n = 30$). For frequency histograms and density traces see Figs. A.1 (ship set) and A.2 (air set).

Transport maturity			Shelf life time (days)					
			0	1	2	5	6	7
Ship	minimum		−3.94	−3.62	−3.54	−1.60	−0.86	−0.58
	maximum		3.45	3.74	4.33	4.89	5.00	5.62
	mean		−0.008	0.46	1.11	2.30	2.61	2.85
	Std dev		1.771	1.779	1.651	1.350	1.266	1.263
	χ^2 goodness-of-fit	statistic	9.0	11.0	6.0	8.8	5.7	13.9
		P-value	0.70	0.53	0.92	0.72	0.93	0.30
	Shapiro Wilks W statistic	statistic	0.9804	0.9651	0.9579	0.9493	0.9419	0.9661
		P-value	0.86	0.46	0.31	0.20	0.13	0.50
Air	minimum		−4.91	−5.07	−2.77	−1.78	−0.51	−0.02
	maximum		4.83	5.21	5.53	6.20	6.43	6.60
	mean		0.063	0.42	1.31	2.64	3.05	3.38
	Std dev		2.388	2.492	2.116	1.785	1.617	1.560
	χ^2 goodness-of-fit	statistic	15.0	10.0	7.0	12.7	12.7	5.21
		P-value	0.24	0.62	0.86	0.39	0.39	0.95
	Shapiro Wilks W statistic	statistic	0.9873	0.9861	0.9716	0.9737	0.9721	0.9721
		P-value	0.97	0.96	0.63	0.71	0.66	0.66

Table 3
BSF for μ_a540 ($\Delta t_{\mu a540}$) for samples d0, d1, d2, d5, d6 and d7 of ship and air data sets: minimum, maximum, mean, standard deviation values of distributions and results of tests for normality ($n = 30$). For frequency histograms and density traces see Figs. A.1 (ship set) and A.2 (air set).

Transport maturity			d0	d1	d2	d5	d6	d7
Ship	minimum		−4.79	−2.78	−1.76	0.08	0.23	−0.58
	maximum		3.95	6.17	3.92	4.71	5.15	5.62
	mean		−0.09	0.51	1.16	2.27	2.68	2.85
	Std dev		1.834	1.810	1.530	1.015	1.168	1.263
	χ^2 goodness-of-fit	statistic	10.0	9.0	7.0	22.4	12.0	13.9
		P-value	0.62	0.70	0.86	0.03	0.44	0.30
	Shapiro Wilks W statistic	statistic	0.9852	0.9510	0.9767	0.9478	0.9851	0.9661
		P-value	0.94	0.21	0.76	0.20	0.94	0.50
Air	minimum		−3.49	−5.39	−2.10	0.48	0.53	−0.02
	maximum		7.31	4.86	5.95	5.91	9.15	6.60
	mean		0.34	0.56	1.41	3.19	3.37	3.38
	Std dev		2.331	2.318	1.974	1.320	1.699	1.560
	χ^2 goodness-of-fit	statistic	6.0	13.0	7.0	18.1	19.0	5.21
		P-value	0.92	0.37	0.86	0.11	0.09	0.95
	Shapiro Wilks W statistic	statistic	0.9598	0.9820	0.9715	0.9775	0.9228	0.9721
		P-value	0.35	0.89	0.62	0.79	0.04	0.66

3. Results

3.1. The μ_a540

The μ_a540 at fruit sorting did not differ between the two transport maturity stages, being (mean ± standard error) 0.157 ± 0.003 cm^{-1} in fruit for ship transport and 0.166 ± 0.004 cm^{-1} for air transport; values were in the 0.103–0.403 cm^{-1} (ship maturity) and 0.106–0.511 cm^{-1} (air maturity) ranges, with a different distribution between the two transport maturities. In fact, considering the ship set, 51% of fruit had μ_a540 values lower than 0.15 cm^{-1}, 35% were in the 0.15–0.19 cm^{-1} interval, 9.6% in the 0.19–0.23 cm^{-1} and 6.2% had μ_a540 higher than 0.23 cm^{-1}. Differently, in the air set 44% of fruit showed μ_a540 lower than 0.15 cm^{-1}, 13% were in the 0.19–0.23 cm^{-1} range and 9% had μ_a540 values higher than 0.23 cm^{-1}.

3.2. The μ_a540 model

With shelf life μ_a540 increased in all fruit showing the largest variation at the end of shelf life (Figs. 4 and 5). Fitting the μ_a540 values of the 30 mangoes of the samples d7 in function of shelf life at 20 °C with the traditional approach of the exponential regression model without considering the BSF approach only about 36% and 28% of the variability, for ship and air transport maturity respectively, could be explained with quite large standard errors of the estimate (>0.2).

To study the μ_a540 increase using the logistic model of Eq. (4) and considering the individual information obtainable by the BSF approach, the rate constant k_m was estimated using the nonlinear regression procedure (Table 1). The k_m was about 0.108 cm^{-1} day^{-1} for the ship set, 0.094 cm^{-1} day^{-1} for air set and 0.1 cm^{-1} day^{-1} for ship+air set with R^2_{adj} in the 78–83% range.

Considering the evolution of BSF of sample d7 fruit of the ship set with shelf life (Table 2), it ranged from −3.94 to 3.45 days at the beginning of shelf life to −0.58 to 5.62 days after 7 days, with the average value increasing from −0.01 days at d0 to 2.85 days at d7 and the standard deviation decreasing from 1.77 at d0 to 1.26 at d7. The distributions of BSF were normal with 99% confidence at χ^2 goodness-of-fit statistic and Shapiro-Wills W statistic (Table 2).

As for the BSF of d7 sample fruit belonging to the air set (Table 2), the minimum values of BSF ranged from about −5 days at the beginning of shelf life to −0.02 days at d7, and the maximum values ranged from 4.83 days at d0 to 6.60 days at d7; the average value increased from 0.06 days at d0 to 3.38 days at d7, with the standard deviation decreasing from 2.39 at d0 to 1.56 at d7. The distributions of BSF were normal with 99% confidence at χ^2 goodness-of-fit statistic and Shapiro-Wills W statistic (Table 2).

Considering the BSF of the samples analyzed for pulp color parameters (Table 3), the minimum values were in the −4.8 - −0.6 days range

Table 4
Modeling of μ_a540 vs $t+\Delta t_{\mu a540}$ of sample d7 data during shelf life: estimates and standard error of intercept and slope of (A) logistic and (B) exponential regression models, R^2_{adj}, SEE and MAE for ship (d.f.=176), air (d.f.=173) and ship+air (d.f.=350) data sets.

	intercept		Slope		R^2_{adj}	SEE	MAE	P-value model
Data set	estimate	SE	Estimate	SE				
A - logistic								
Ship	−1.6985***	0.0009	0.0610***	0.0021	99.9	0.0087	0.0064	<0.0001
Air	−1.7051***	0.0009	0.0566***	0.0001	99.9	0.0092	0.0069	<0.0001
ship+air	−1.7011***	0.0009	0.0585***	0.0001	99.9	0.0129	0.0099	<0.0001
B - exponential								
Ship	−1.8656***	0.0018	0.0484***	0.0002	99.6	0.0175	0.0123	<0.0001
Air	−1.8710***	0.0020	0.0446***	0.0002	99.5	0.0196	0.0143	<0.0001
ship+air	−1.8676***	0.0015	0.0462***	0.0002	99.4	0.0204	0.0145	<0.0001

Table 5
Modeling of μ_a540 vs $t+\Delta t_{\mu a540}$ using data of samples d0, d1, d2, d5, d6 and d7: estimates and standard error of intercept and slope of (A) logistic and (B) exponential regression models, R^2_{adj}, SEE and MAE for ship (d.f.=176), air (d.f.=176) and ship+air (d.f.=353) data sets.

	intercept		slope		R^2_{adj}	SEE	MAE	P-value model
Data set	estimate	SE	estimate	SE				
A - logistic								
Ship	−1.6206***	0.0008	0.0669***	0.0001	99.9	0.0091	0.0063	<0.0001
Air	−1.6035***	0.0038	0.0644***	0.0005	98.8	0.0411	0.0140	<0.0001
Ship+air	−1.6960***	0.0011	0.0556***	0.0001	99.8	0.0146	0.0099	<0.0001
B - exponential								
ship	−1.8016***	0.0018	0.0524***	0.0003	99.4	0.0199	0.0134	<0.0001
Air	−1.7853***	0.0013	0.0490***	0.0002	99.8	0.0136	0.0102	<0.0001
Ship+air	−1.8557***	0.0025	0.0424***	0.0003	98.5	0.0340	0.0205	<0.0001

for the ship set and in the −3.5 - −0.02 days range for the air set, while the maximum values ranged from 3.9 days (samples d0 and d2) to 5.6 days (sample d7). The mean values increased from −0.1 (sample d0) to 2.8 days (sample d7) for the ship set and from 0.3 (sample d0) to 3.4 days (sample d7) for the air set, with standard deviation decreasing with shelf life from 1.83 to 1.26 in the ship set and from 2.33 to 1.56 in the air set. All the distributions of BSF for the ship set were normal with 99% confidence at Shapiro-Wills W statistic, and, except for sample d5, at χ^2 goodness-of-fit statistic. In contrast, all the distributions of BSF for the air set were normal with 99% confidence at χ^2 goodness-of-fit statistic and, except for sample d6, at Shapiro-Wills W statistic (Table 3). The frequency histograms and density traces of BSF of ship set belonging to d7 sample and to samples analyzed for color parameters shown in Fig. A.1 compared with those of air set reported in Fig. A.2 confirm the similarity of the BSF evolution in shelf life of the six samples from both data sets, as well as underline the differences between the two transport maturities, with air set having a wider range of BSF than the ship set.

As for the regression analysis of μ_a540 vs $t+\Delta t_{\mu a540}$, for each data set both the logistic and the exponential models were considered (Tables 4 and 5; Fig. 6) From Fig. 6 it can be seen that considering the individual differences in maturity by BSF, the μ_a540 values of Fig. 5 are shifted following the same curve, highlighting that each individual fruit represents a step in the same process.

The R^2_{adj} of all the models were higher than 99.0% for both logistic and exponential models.

3.3. Mesocarp color

Mesocarp color parameters during shelf life did not differ between the two transport maturity stages (Table 6). With shelf life, L^* and h° decreased, while a^*, b^*, C^* and I_Y increased, with the main changes occurring from d2 and d5 for both the transport maturities. Except for L^* of ship set, which further decreased till the end of shelf life, L^* of air set and a^*, b^*, C^*, h° and I_Y of both sets did not further change with time of shelf life.

3.4. Color parameters models

For each transport maturity stage, the L^*, a^*, b^*, C^*, h° and I_Y values of the 30 mangoes of each sample were plotted in function of shelf life at 20 °C, expressed as calendar time (days) and fitted with the regression model having the best performance (higher R^2_{adj}, lower SEE and MAE), without considering the BSF approach (Fig. B.1a and b). Raw data showed a large variation for all the color parameters, with a percentage variance explained ranging from 33 to 50%.

Aiming at modeling pulp color parameters in function of the BSF approach, the coefficient of the independent variable μ_a540 (α_{540}) and the β parameter of the Eq. (9) were estimated, along with the rate constant k_m, by the nonlinear regression procedure, adopting model (6) for b^*, C^* and I_Y, model (7) for $a^*$and model (8) for L^* and h° combined with Eq. (9), in which the δ value decreases with the increase of the shelf life time from 0.773±0.024 at d0 to 0.488±0.021 at d7, and increases with the increase of ranking order in the samples (i.e., decreasing maturity) from 0.126±0.072 for Rank 1 to 0.905±0.049 for Rank 30. The results of the estimates of the models' parameters for each data set are reported in Table 7; Fig. 7 shows for each color parameter the estimated response surfaces, i.e., the predicted values in function of time of shelf life expressed in normalized days and δ, and the plots predicted vs. observed for the ship+air set.

To avoid over parameterization, the minimum and maximum values have been fixed at the minimum and maximum values ever measured in this and previous our experiments on mango fruit, and these values were used for all the data sets. Generally, the R^2_{adj} of the models was >90%, with higher values for I_Y (96.5–99.1%) and h° (96.3–99.8%) than the R^2_{adj} for L^* (94–97%), a^* (94.4–99.3%), b^* (93–99%) and C^* (91.8–97.4%).

The rate constant k_m depended on the color parameter and/or the transport maturity (Table 7). Whatever the data set, the k_m for L^* and h° showed higher values than the other color parameters, being, respectively, in the 0.9–1.1 and 0.4–0.8 ranges; b^* and I_Y showed the lowest k_m values, being in the 0.14–0.18 and 0.12–0.15 ranges, respectively. Comparing the two transport maturities, the k_m of L^* and b^* were significantly higher and those of I_Y and h° were significantly lower in the

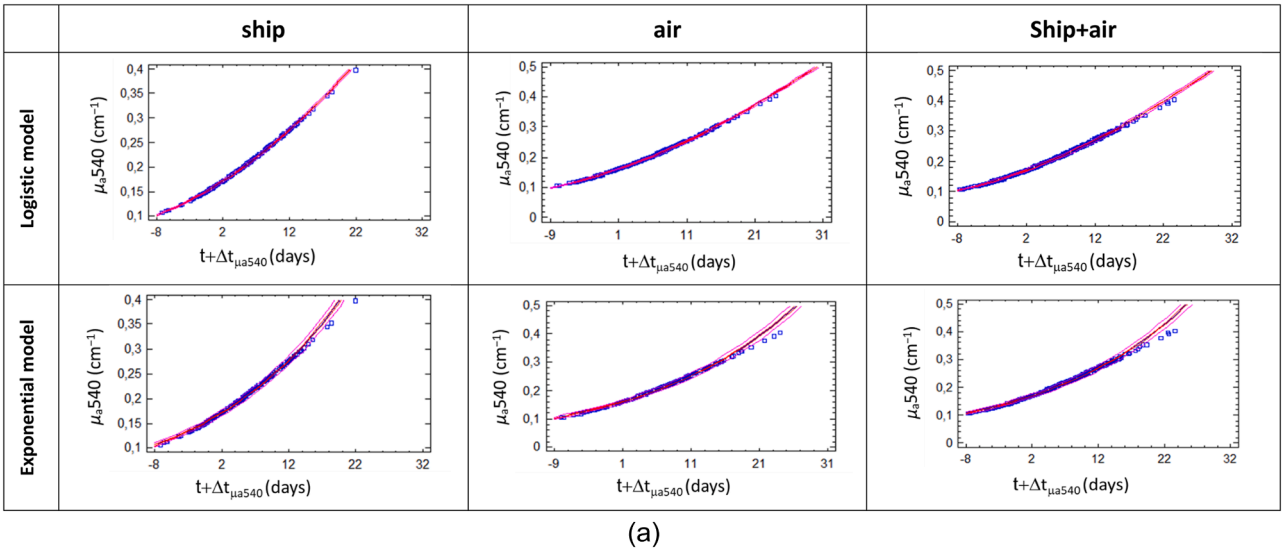

Fig. 6. Measured (symbols) and predicted (lines) μ_a540 in function of BSF ($t+\Delta t_{\mu a540}$) for sample d7 data (panel a) for samples d0, d1, d2, d5, d6 and d7 data (panel b) of ship (left), air (center) and ship+air (right) sets by logistic (top) and exponential (bottom) models, Models' details are reported in Tables 4 and 5.

air set.

The BSFs, expressed in normalized time, differed among color parameters and between transport maturities (Table 8). All the BSFs distributions were normal according to χ^2 goodness-of-fit and Shapiro Wilks W statistic tests (data not shown). The BSFs of ship transport maturity fruit related to L^*, a^*, h° and I_Y (Table 8) were lower than those observed for air transport maturity fruits, while the BSFs related to b^* and C^* were higher. Negative values from −0.96 to −0.20 normalized days (norm d) were observed for Δt_{L^*} for almost all the fruit of both ship and air transport maturities and for Δt_{a^*} for some fruit of the ship set. Low but positive values from 0.02 to 0.69 norm d were found for Δt_{H° for all the fruit of both the transport maturities. The ranges of Δt values of the other color parameters were: 4.33–7.86 norm d for Δt_{IY}, 5.16–9.55 norm d for Δt_{b^*} and 9.17–15.74 norm d for Δt_{C^*} (Table 8).

Considering the shelf-life time (Tables 10–15), in all the sets the minimum BSFs values were observed at the beginning of shelf life, then they increased significantly from d0 to d2 (only ship and ship+air sets) and from d2 to d5, then they did not change till the end of shelf life.

Table 9 and Fig. 8 (ship+air set) report the results of regression analysis of color parameters vs the specific biological shift factor (Δt_y) for ship, air, and ship+air sets.

The type and the performance of regression model of Δt_y vs the y color parameter depends on color parameters and on two transport maturities, with R^2_{adj} ranging from 73 to 86%.

4. Discussion

4.1. The μ_a540

The μ_a540 was used as the non-destructive maturity index to sort fruit at arrival from the most mature (highest value in the batch) to the least mature (least value in the batch). The μ_a540 was also used to obtain for each fruit its biological age expressed as biological shift factors specific for μ_a540 and for L^*, a^*, b^*, C^*, h° and I_Y color parameter, as each fruit at the time of examination had undergone a more or less advanced stage of the ripening process related to the specific property.

The μ_a540 showed similar values to those reported for the same cultivar (Vanoli et al., 2013) and for other mango cultivars (Vanoli et al., 2018), and increased with the shelf-life time for both the transport maturities, in agreement with Vanoli et al. (2013)'s findings even if the correlation was very low with day of shelf life. This low correlation could be due to the fact that fruit had been picked at a ripening degree

Table 6
Mesocarp color parameters L^*, a^*, b^*, chroma (C^*), hue (h°) and Yellowness Index (I_Y) of d0, d1, d2, d5, d6 and d7 samples of ship and air transport maturity degrees at harvest.

Shipping maturity			d0	d1	d2	d5	d6	d7
ship	L^*	mean	82.7 a	81.5ab	81.0 b	78.8 c	77.6 cd	77.0 d
		SE	0.34	0.56	0.33	0.34	0.41	0.38
	a^*	mean	−0.32 c	1.53 bc	2.58 b	5.41 a	6.05 a	6.29 a
		SE	0.56	0.54	0.49	0.36	0.35	0.35
	b^*	mean	52.3 c	54.0 bc	56.5 b	60.5 a	60.5 a	61.2 a
		SE	0.93	0.75	0.79	0.66	0.48	0.61
	C^*	mean	52.4 c	54.1 bc	56.6b	60.7 a	60.8 a	61.5 a
		SE	0.93	0.77	0.81	0.68	0.50	0.63
	h°	mean	90.7 a	88.6 a	87.6 a	85.0 b	84.3 b	84.2 b
		SE	0.61	0.54	0.47	0.30	0.30	0.31
	I_Y (%)	mean	113.0 c	120.1 bc	127.1 b	142.1 a	145.0 a	147.8 a
		SE	2.93	2.86	2.63	2.26	2.02	2.15
Air	L^*	mean	80.5 a	82.0 ab	80.2 b	77.6 c	77.1 c	76.3 c
		SE	0.49	0.33	0.43	0.32	0.53	0.55
	a^*	mean	0.38 b	1.41 b	2.51 b	6.24 a	6.34a	6.79 a
		SE	0.74	0.59	0.67	0.35	0.47	0.46
	b^*	mean	52.9 c	54.3 bc	56.9 b	61.3 a	60.9 a	61.9 a
		SE	1.17	0.95	0.88	0.37	0.54	0.56
	C^*	mean	53.1 c	54.4 bc	57.0 b	61.6 a	61.3 a	62.3 a
		SE	1.18	0.96	0.89	0.39	0.58	0.59
	h°	mean	90.71 a	88.8 a	87.8 a	84.2 b	84.1 b	83.8 b
		SE	0.78	0.62	0.66	0.31	0.39	0.39
	I_Y (%)	mean	115.5 c	120.0 bc	129.2 b	146.9 a	147.4 a	151.6 a
		SE	3.84	3.00	3.14	1.536	2.68	2.48

Means followed by different letters are statistically different (Tukey's test, $P<0.001$).

Table 7
Parameters of the non-linear regression models for L^*, a^*, b^*, chroma (C^*), hue (h°) and yellowness index (I_Y) pulp color parameters in function of μ_a540 for ship (d.f.=176), air (d.f.=176) and ship+air (d.f.=353) mango fruit sets, R^2_{adj}, SEE and MAE of the models.

			L^*	a^*	b^*	C^*	h°	I_Y
	model		8	7	6	6	8	6
	minimum [a]		60	−10	30	35	75	70
	maximum [a]		87	14	75	70	105	200
ship	k_m	estimate	0.9181	0.2558	0.1369	0.1608	0.7894	0.1464
		Approx. S.E.	0.0423	0.0144	0.0066	0.0097	0.0079	0.0063
	α_{540}	estimate	−12.8398	−14.8329	−13.5293	−18.0435	−2.7443	−45.3835
		Approx. S.E.	3.1158	3.6176	3.6596	4.4900	0.7448	10.7447
	β	estimate	−9.0967	9.0219	58.972	63.4999	3.7167	134.215
		Approx. S.E.	1.5051	2.6815	2.5294	3.1099	0.5862	6.2778
	R^2_{adj}		95.2	95.5	93.0	91.8	99.8	96.5
	SEE		0.6540	0.7427	1.3784	1.5208	0.1690	3.5132
	MAE		0.4642	0.3566	0.7436	0.9460	0.1081	1.8415
	P-value		<0.0001	<0.0001	<0.0001	<0.0001	<0.0001	<0.0001
air	k_m	estimate	1.1505	0.2331	0.1808	0.1833	0.4667	0.1263
		Approx. S.E.	0.0351	0.0045	0.0029	0.0057	0.0056	0.0025
	α_{540}	estimate	−3.3182	−3.1229	−6.7916	−12.7126	−4.1982	−21.9897
		Approx. S.E.	2.2868	1.5506	1.3764	2.6492	0.9152	5.6509
	β	estimate	−7.8176	8.6503	49.6724	56.507	7.8205	119.103
		Approx. S.E.	0.9895	0.9877	1.0143	1.9339	0.9152	3.3656
	R^2_{adj}		97.0	99.3	99.0	97.4	99.6	99.1
	SEE		0.5932	0.3339	0.5509	0.9142	0.2331	1.9915
	MAE		0.4563	0.2088	0.4249	0.7069	0.1598	1.3198
	P-value		<0.0001	<0.0001	<0.0001	<0.0001	<0.0001	<0.0001
Ship+air	k_m	estimate	0.9427	0.1580	0.1434	0.1631	0.4338	0.1224
		Approx. S.E.	0.0318	0.0078	0.0044	0.0058	0.0135	0.0034
	α_{540}	estimate	−14.0887	−33.1397	−16.3537	−19.1813	−21.3988	−55.2112
		Approx. S.E.	2.2084	2.4416	2.3043	2.7463	1.8251	6.7867
	β	estimate	−6.1409	25.3498	59.1752	62.8968	20.0264	138.508
		Approx. S.E.	1.0154	1.6674	1.6393	1.9534	1.3699	4.0394
	R^2_{adj}		94.4	94.4	94.3	94.0	96.3	97.1
	SEE		0.7666	0.8849	1.2910	1.3485	0.7066	3.4290
	MAE		0.5983	0.6317	0.8510	0.9278	0.5559	2.3563
	P-value		<0.0001	<0.0001	<0.0001	<0.0001	<0.0001	<0.0001

[a] fixed values; α_{540} is the coefficient of the independent variable μ_a540.

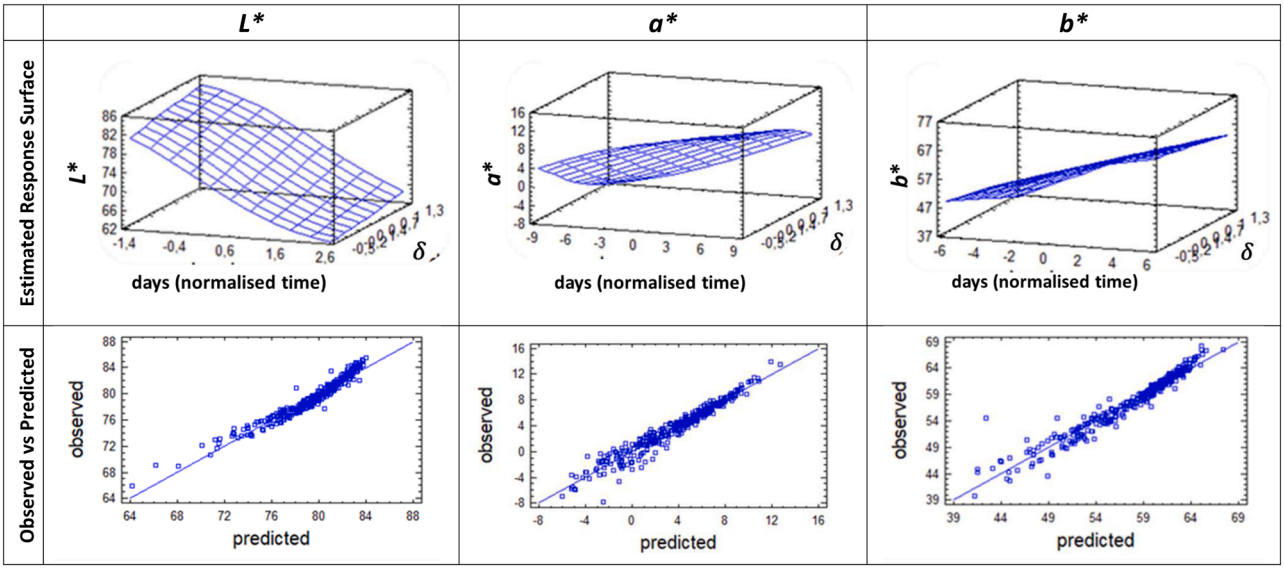

Fig. 7. Estimated response surface (top) and plot of predicted vs observed (bottom) by non-linear regression models for lightness (L^*), a^* and b^* pulp color parameters (panel a) and for chroma (C^*), hue and yellowness index (I_Y) pulp color parameters (panel b) of ship+air set. See Table 7 for models' parameters.

Table 8
BSF for pulp color parameters (Δt) of ship and air data sets: minimum, maximum, mean, standard deviation values of distributions ($n = 177$).

Transport maturity		L^*	a^*	b^*	C^*	h°	I_Y
ship	minimum	−0.96	−1.29	7.06	10.66	0.02	4.33
	maximum	−0.37	1.44	9.55	15.74	0.16	7.02
	mean	−0.70	−0.07	8.17	12.93	0.08	5.53
	Std dev	0.099	0.462	0.420	0.858	0.022	0.456
air	minimum	−0.37	0.91	5.16	9.17	0.22	5.73
	maximum	−0.20	1.80	6.48	13.57	0.69	7.86
	mean	−0.32	1.20	5.59	10.63	0.37	6.43
	Std dev	0.023	0.122	0.183	0.605	0.065	0.292

more advanced than the preclimacteric mature-green stage, in order to have better quality at consumption, as shown by I_Y values greater than 100 at the beginning of shelf life This means that a certain amount of carotenoids was present in the pulp, which can further improve with shelf life day only in little quantities, as most likely both experiments started when carotenoid content fell in the last part of the logistic curve of carotenoid synthesis. Notwithstanding that on average the μ_a540 did not differ between the two transport maturities, differences still exist

Table 9
Results of regression analysis between BSF and pulp color parameters for ship, air and ship+air sets: estimates and standard error of intercept and slope of regression models, R^2_{adj}, SEE and MAE. MT=model type (*L*=linear; *M*=multiplicative; RX=reciprocal-X; RY=reciprocal-Y; *Sc*=*S*-curve; SqrY=square root-Y).

set			*L**	*a**	*b**	*C**	*h*°	I_Y
Ship	MT		L	L	Sc	Sc	RY	Sc
	intercept	estimate	60.6979	4.0642	5.6380	5.3126	0.0100	6.5244
		S.E.	0.6956	0.1028	0.0681	0.0509	5.15E−5	0.0511
	slope	estimate	−27.3782	6.9825	−12.8917	−16.2573	0.0183	−9.0631
		S.E.	0.9874	0.2202	0.5545	0.6541	6.0E−4	0.2800
	R^2_{adj} (%)		81.3	85.1	75.4	77.8	84.1	85.6
	SEE		1.2962	1.3473	0.0463	0.0448	1.76E−4	0.0561
	MAE		1.0339	0.9935	0.0345	0.0338	1.31E−4	0.0445
	P-value		<0.0001	<0.0001	<0.0001	<0.0001	<0.0001	<0.0001
Air	MT		RY	RX	RX	RX	M [a]	RX
	intercept	estimate	0.0194	41.2778	206.665	148.215	4.2251	569.124
		S.E.	2.73E−4	1.0979	6.7817	3.6806	0.0076	13.9408
	slope	estimate	0.0213	−44.5642	−830.723	−953.352	−0.2350	−2089.36
		S.E.	8.59E−4	1.3026	37.8689	38.9339	0.0075	89.4435
	R^2_{adj} (%)		77.8	86.9	73.2	77.3	84.7	84.7
	SEE		2.66E−4	1.4437	2.8865	2.7242	0.0174	8.2489
	MAE		2.14E−4	1.0961	2.1515	2.0606	0.0125	6.5733
	P-value		<0.0001	<0.0001	<0.0001	<0.0001	<0.0001	<0.0001
Ship+air	MT		SqrY	L	RX	RX	RY	RX
	intercept	estimate	8.0783	3.0713	127.048	121.793	0.0109	303.568
		S.E.	0.0023	0.0792	2.0744	1.7916	1.88E−5	3.7529
	slope	estimate	−1.4294	1.6731	−523.79	−792.23	0.0013	−1097.65
		S.E.	0.0388	0.0378	15.627	22.163	3.07E−5	24.0885
	R^2_{adj} (%)		79.3	84.8	76.1	78.3	83.2	85.5
	SEE		0.0828	1.4631	2.6370	2.5701	1.94E−4	7.6279
	MAE		0.0669	1.0700	1.9850	1.9557	1.40E−4	6.0694
	P-value		<0.0001	<0.0001	<0.0001	<0.0001	<0.0001	<0.0001

[a] ln (H)=intercept – slope*ln($BSF_{H°}$).

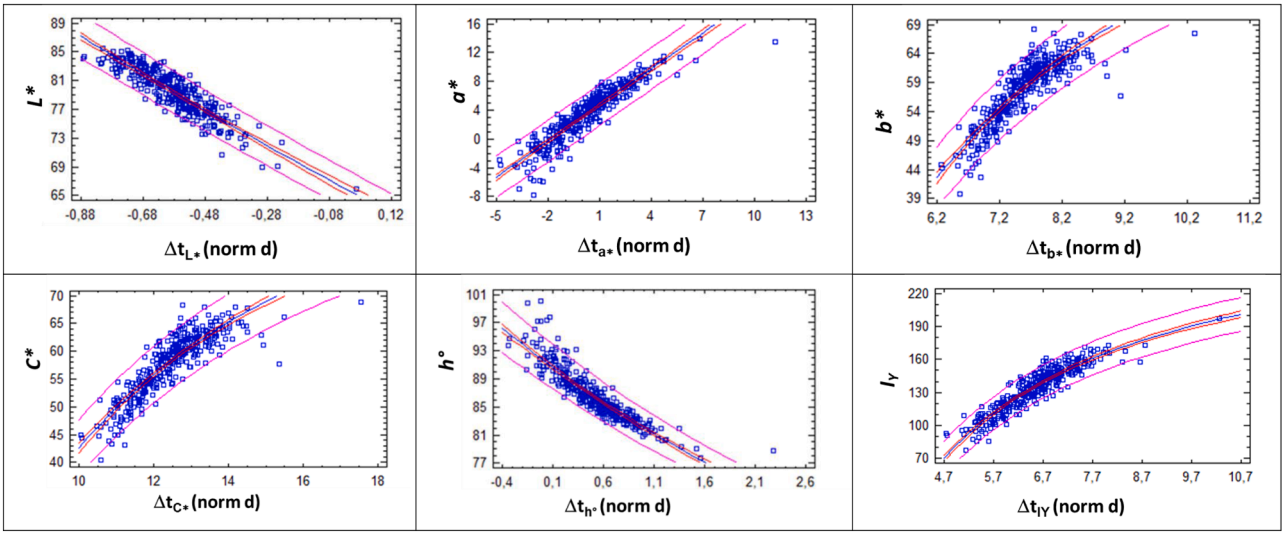

Fig. 8. Lightness (*L**), *a**, *b** (top), chroma (*C**), hue and Yellowness Index (I_Y) (bottom) pulp color parameters of ship+air set in function of the specific BSF Δt, fitted with the model having higher performance (for details see Table 9) (blue line), confidence limits at 95% level (inner red lines), prediction limits (outer red lines) and experimental data (symbols). (For interpretation of the references to colour in this figure legend, the reader is referred to the web version of this article.)

between the two mango lots: the range of μ_a540 values at sorting of ship transport maturity was narrower (0.3 cm^{-1}) than that of air transport maturity (0.405 cm^{-1}), with 51% of fruit being less mature (μ_a540 < 0.15 cm^{-1}) and 15.8% of fruit being more mature (μ_a540>0.19 cm^{-1}) vs 44% of fruit with μ_a540< 0.15 cm^{-1} and 21% with μ_a540>0.19 cm^{-1}.

4.2. Mesocarp color parameters

The values of pulp color parameters and their behavior in shelf-life were like those reported for 'Tommy Atkins' mangoes from Brazil in our previous works (Vanoli et al., 2013; Vanoli et al., 2011; Rizzolo et al., 2011) and in the literature (De Morais et al., 2002; Sabato et al., 2009; de Mello Vasconcelos et al., 2019).

During ripening mesocarp color turned from greenish-yellow to orange, as *a**, *b**, *C** and yellowness index (I_Y) increased and *h*° decreased with shelf life (De Morais et al., 2002; Dang et al., 2008; Ornelas-Paz et al., 2008; Vásquez-Caicedo et al., 2006; Vanoli et al., 2011 and 2013; Rizzolo et al., 2011; Spinelli et al., 2012; Candelario-Rodríguez et al., 2014; Gill et al., 2017). Lightness (*L**) decreased with ripening due to changes in fruit texture rather than to pigment contents (De Morais

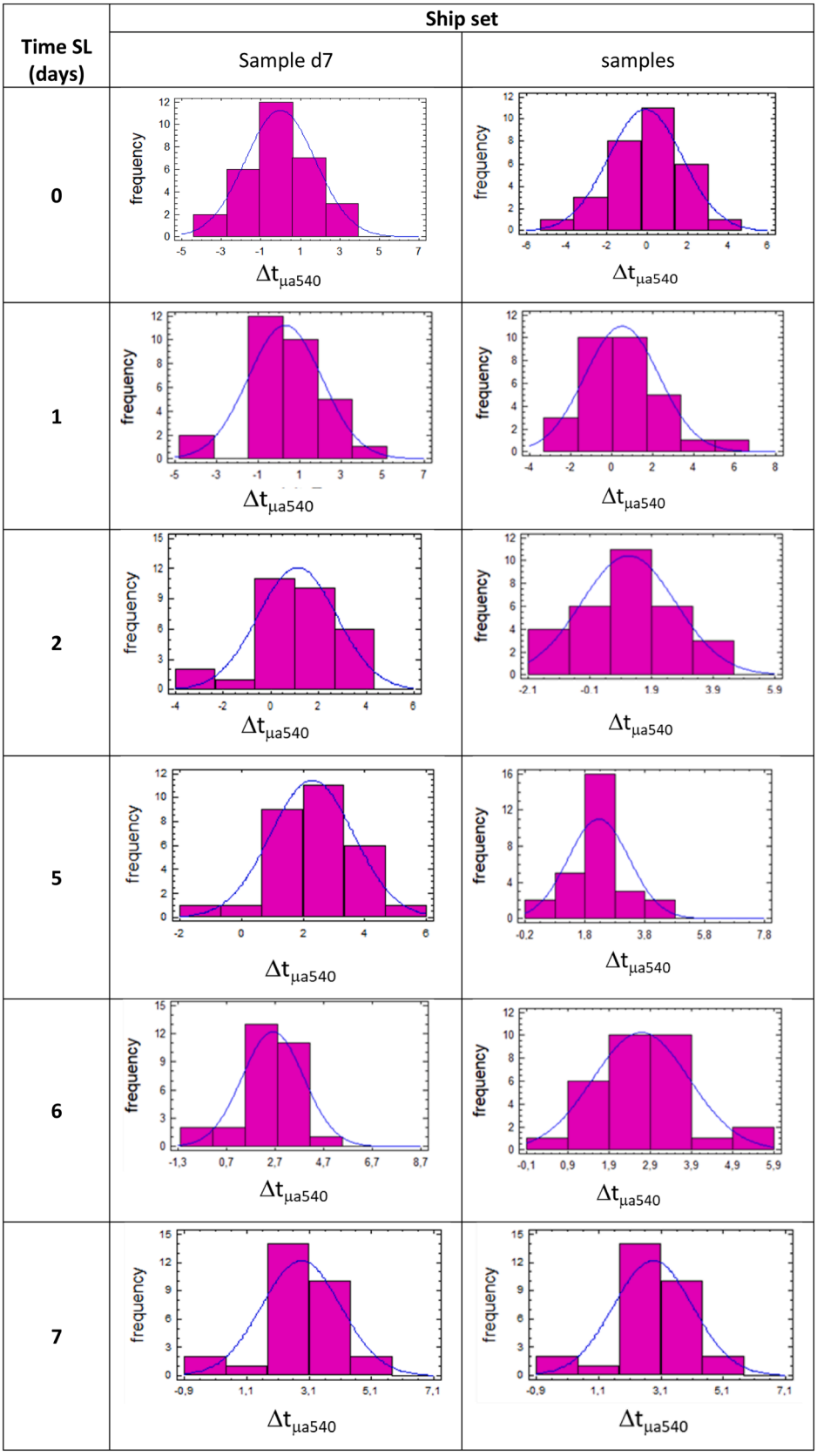

Fig. A.1. Ship transport maturity set: Frequency histograms and density traces of BSF for μ_a540 ($\Delta t_{\mu a540}$) of sample d7 data in shelf life (left) and of d0, d1, d2, d5, d6 and d7 samples (right).

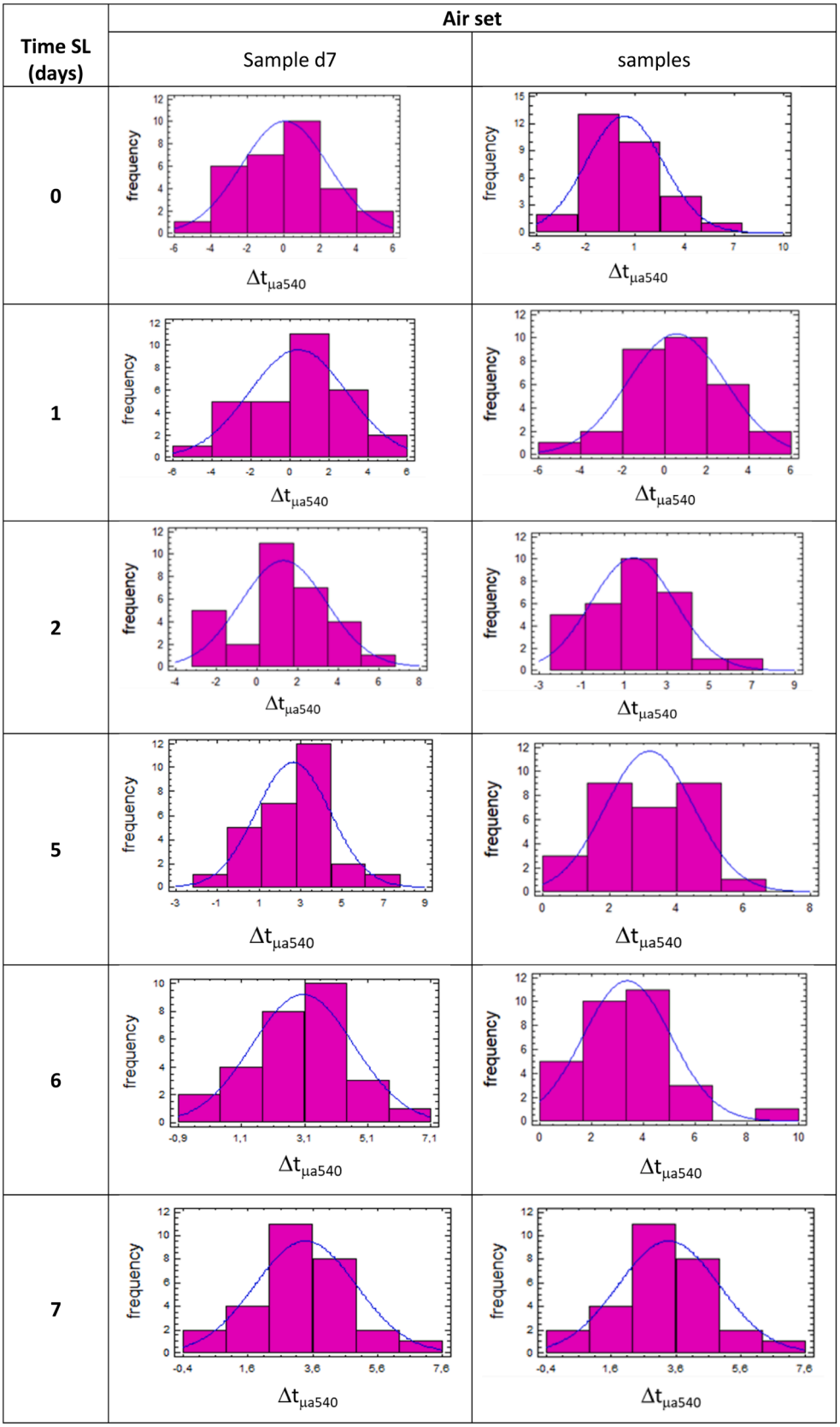

Fig. A.2. Air transport maturity set: Frequency histograms and density traces of BSF for μ_a540 ($\Delta t_{\mu a540}$) of sample d7 data in shelf life (left) and of d0, d1, d2, d5, d6 and d7 samples (right).

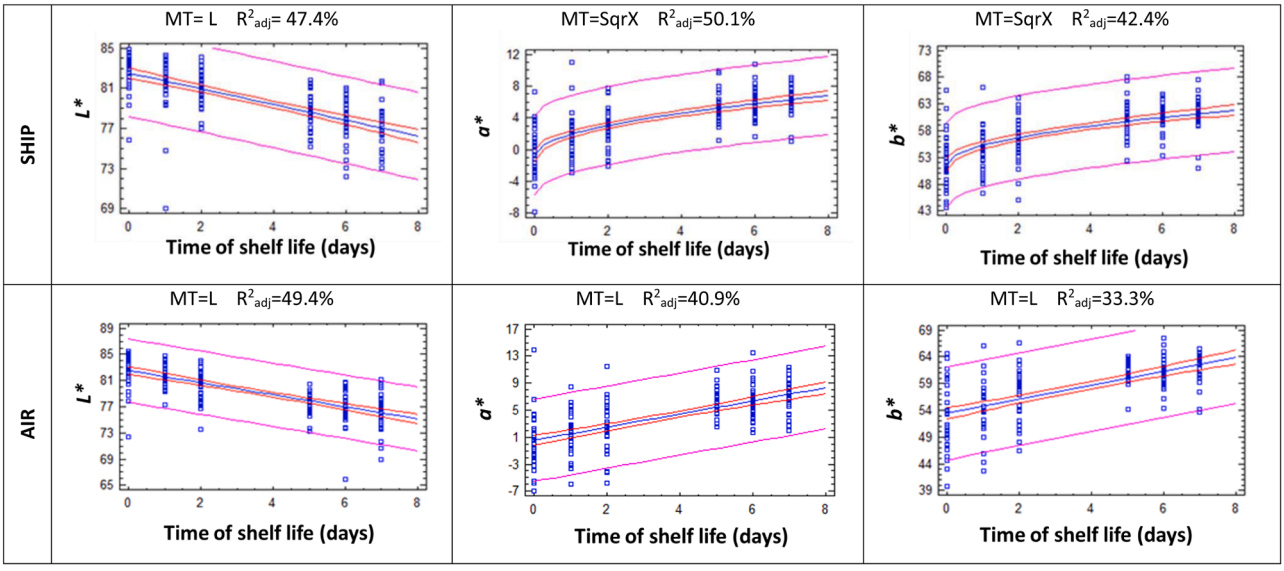

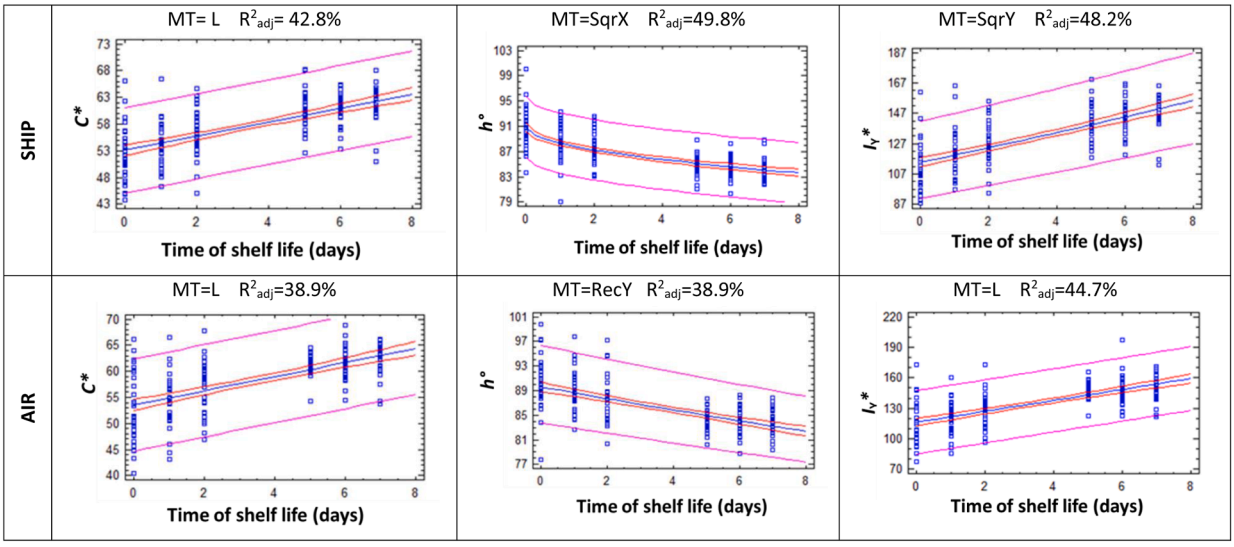

Fig. B1.a. Panel a: Lightness (L^*), **a*** and b^* pulp color parameters of ship (top) and air (bottom) transport maturities in function of time of shelf life at 20°C, fitted with model having higher performance, confidence limits at 95% level (inner lines), prediction limits (outer lines) and experimental data (symbols), model type and R-squared adjusted for d.f. (R^2_{adj}). MT=model type (L=linear; SqrX=square root-X). All models have P-value <0.0001. Panel b: Chroma (C^*), hue and Yellowness Index (I_Y) pulp color parameters of ship (top) and air (bottom) transport maturities in function of time of shelf life at 20°C, fitted with model having higher performance, confidence limits at 95% level (inner lines), prediction limits (outer lines) and experimental data (symbols), model type and R-squared adjusted for d.f. (R^2_{adj}). MT=model type (L=linear; RecY=reciprocal-Y; SqrX=square root-X; Sqr-Y=square root-Y). All models have P-value <0.0001.

Table 10
BSF (norm d) for L^* (Δt_{L^*}) of ship+air data set in function of shelf-life time at 20 °C: minimum, maximum, mean, and standard deviation values of distributions.

	d0	d1	d2	d5	d6	d7
N.	60	60	60	57	60	57
minimum	−0.87	−0.87	−0.77	−0.68	−0.66	−0.72
maximum	−0.23	−0.25	−0.35	−0.35	0.01	−0.30
Mean	−0.67	−0.65	−0.62	−0.54	−0.52	−0.51
Std dev	0.105	0.105	0.091	0.072	0.102	0.086

Table 11
BSF (norm d) for a^* (Δt_{a^*}) of ship+air data set in function of shelf-life time at 20 °C: minimum, maximum, mean, and standard deviation values of distributions.

	d0	d1	d2	d5	d6	d7
N.	60	60	60	57	60	57
minimum	−4.82	−4.74	−2.93	−1.36	−1.22	−1.94
maximum	6.83	6.56	4.70	4.65	11.20	5.66
mean	−1.16	−0.79	−0.16	1.23	1.63	1.70
Std dev	1.904	1.911	1.658	1.305	1.858	1.557

et al., 2002; Vanoli et al., 2011, 2013; Gill et al., 2017; Penchaia et al., 2020). Rizzolo et al. (2011) found that the rate of color changes with shelf life in 'Tommy Atkins' mangoes was different in fruit classified as less, medium and more mature according to μ_a630: h° decreased and I_Y increased with the highest rate for less mature class and the least rate for more mature class, and L^* decreased faster in medium and more mature

Table 12
BSF (norm d) for b^* (Δt_{b^*}) of ship+air data set in function of shelf-life time at 20 °C: minimum, maximum, mean, and standard deviation values of distributions.

	d0	d1	d2	d5	d6	d7
N.	60	60	60	57	60	57
minimum	6.27	6.29	6.75	7.14	7.18	7.00
maximum	9.21	9.14	8.67	8.66	10.31	8.92
mean	7.19	7.29	7.45	7.80	7.90	7.92
Std dev	0.479	0.482	0.418	0.329	0.469	0.392

Table 13
BSF (norm d) for C^* (Δt_{C^*}) of ship+air data set in function of shelf-life time at 20 °C: minimum, maximum, mean, and standard deviation values of distributions.

	d0	d1	d2	d5	d6	d7
N.	60	60	60	57	60	57
minimum	10.04	10.08	10.92	11.66	11.73	11.39
maximum	15.49	15.36	14.49	14.47	17.54	14.94
mean	11.75	11.92	12.22	12.87	13.06	13.09
Std dev	0.890	0.894	0.775	0.610	0.869	0.728

Table 14
BSF (norm d) for h° (Δt_{H°) of ship+air data set in function of shelf-life time at 20 °C: minimum, maximum, mean, and standard deviation values of distributions.

	d0	d1	d2	d5	d6	d7
N.	60	60	60	57	60	57
minimum	−0.34	−0.33	−0.03	0.22	0.25	0.13
maximum	1.56	1.52	1.21	1.21	2.28	1.37
mean	0.26	0.32	0.42	0.65	0.72	0.72
Std dev	0.311	0.313	0.271	0.213	0.304	0.254

Table 15
BSF (norm d) for I_Y (Δt_{IY}) of ship+air data set in function of shelf-life time at 20 °C: minimum, maximum, mean, and standard deviation values of distributions.

	d0	d1	d2	d5	d6	d7
N.	60	60	60	57	60	57
minimum	4.73	4.76	5.38	5.92	5.98	5.73
maximum	8.76	8.65	8.02	8.00	10.26	8.35
mean	5.99	6.12	6.34	6.82	6.96	6.98
Std dev	0.657	0.659	0.572	0.450	0.641	0.537

classes than in less mature ones.

4.3. Modeling

It has been previously shown that the maturity indices based on the absorption coefficients non-destructively measured by TRS are correlated to mesocarp color parameters (Rizzolo et al., 2011; Vanoli et al., 2011, 2013, 2018; Spinelli et al., 2012), which depends on the main pigment concentrations, i.e., chlorophylls and carotenoids.

Eccher Zerbini et al. (2015) reported that the optical absorptions showed a clear sequence in mango fruit: the increase of μ_a540 (linked to carotenoids) occurred only after the complete decrease of μ_a670 (linked to chlorophyll). Similarly, upon ripening, carotenoids are accumulated in the mesocarp with an exponential behavior, only when chlorophyll is very low or undetectable (Kienzle et al., 2011, 2012). Previously, for 'Palmer', 'Haden' and 'Tommy Atkins' cultivars, positive correlations were found among μ_a540 and a^*, b^* and I_Y, and negative correlation between μ_a540 and h° and L^* (Spinelli et al., 2012; Vanoli et al., 2013, 2016, 2018).

Basing on the close relationship between μ_a540 and carotenoid content, the production model reported in Eq. (4) seems to be appropriate to describe the μ_a540 increase with ripening.

The μ_a670 alone or in combination with μ_a540 and scattering parameters have been so far used to model softening and ethylene production of mangoes (Pereira et al., 2010; Eccher Zerbini et al., 2015), by integrating the BSF derived from the μ_a with firmness decay or ethylene production. In these models, the BSF for μ_a and the BSF for firmness and ethylene should be linearly related according to the Eq. (9) reported in Section 2.3, with α_{540} being the synchronization factor between the ratio of μ_a and firmness or ethylene and β representing the harvest date expressed as a shift factor relative to the midpoint of the curves (Tijskens et al., 2007a).

In this work also for color parameters it was assumed that μ_a540 increase and a^*, b^*, C^*, I_Y increase or L^* and h° decrease are synchronized, and, hence, $\Delta t_{\mu a540}{}^*$ and $\Delta t_y{}^*$ should be related according to Eq. (9). In order to estimate α_{540} and the β parameter of the Eq. (9), the increasing behavior of b^*, C^* and I_Y has been approximated to the sigmoid curve model reported in Eq. (6), that of a^* to the model reported in Eq. (7), whilst the decreasing trends of L^* and h° have been approximated by the model reported in Eq. (8).

4.3.1. The μ_a540 modeling

Two models for μ_a540 as a function of biological time have been studied: logistic and exponential. The logistic model has already been adopted to describe the μ_a670 and the μ_a630 decays in nectarines (Tijskens et al., 2006, 2007b) and in mangoes (Pereira et al., 2010), respectively. The exponential model was also studied, as μ_a540 was linearly correlated with total carotenoids which accumulate in the mesocarp with an exponential behavior during ripening (Vásquez-Caseido et al., 2006; Ornelas-Paz et al., 2008).

The explained parts are very high: 98.8–99.9% for the logistic models and around 98.5–99.8% for the exponential models. The biological shift factor (BSF) showed lower values for the ship set and higher values for the air set, indicating that the fruit of the ship set are less ripe than those of the air set with about a difference of 0.5–1 day. This pattern means that, notwithstanding the mean μa540 value of the two fruit sets was not different at the start of the experiment, there was an influence of the shipping maturity on the behavior with shelf life.

Moreover, the rate constant was slightly lower in the air set respect to the ship set, and the standard deviations of the BSF were slightly higher in the air set. In apples, Rizzolo et al. (2021) observed higher rate constant in less mature fruit than in more mature ones during maturation on the tree. Also, the standard deviation of the BSF was slightly higher in the air set than in the ship one, further confirming an influence of the shipping maturity on fruit ripeness. In fact, all the variation in the BSF is the result of the biochemical changes occurring during fruit growth and ripening at the tree, in the orchard conditions (Tijskens et al., 2007b).

4.3.2. The modeling of color parameters

With μ_a540 and time as independent variables, the explained parts of the non-linear regression models are high for all the fruit sets, being the R^2_{adj} in the 91.8–99.8% range for the ship set, from 97 to 99.6 for the air set and in the 94–97.1 interval for the ship+air set, indicating that almost all variation present in each data set was properly taken care of. The values of constant rates (k_m) for a^*, b^*, C^* and I_Y are not too different from the constant rates found for μ_a540, whereas the estimates for h° and L^* are about three-four times than the k_m values observed for the other color parameters and for μ_a540. The similar k_m values for a^*, b^*, C^* and I_Y could be due to their high correlation to carotenoid content, which in turn, is positively correlated to μ_a540 (Vanoli et al., 2016, 2018). The higher k_m found for h°, which was shown to be highly correlated in mangoes to μ_a630, linked to chlorophyll content (Rizzolo et al., 2011) and to μ_a540 (Vanoli et al., 2018), could suggest that h° value depends on chlorophyll *b*reakdown and on carotenoid

accumulation which are little overlapping and almost mutually exclusive, so that, depending on the fruit age, either one is prevalent (Eccher Zerbini et al., 2015). L^* showed the highest values of k_m as it is mainly influenced by changes in texture and not by pulp pigment dynamics. Changes in texture bound to mango softening have been previously modeled considering the BSF approach by using either μ_a630 for 'Tommy Atkins' fruit during shelf life (Pereira et al., 2010) or μ_a540, μ_a670 and the equivalent size of the scattering centers (Mie's B parameter) on 'Haden' fruit (Eccher Zerbini et al., 2015), obtaining in the first case a k_m value for firmness decay of 0.004, far from those observed for L^* in this work. Hence, it can be envisaged that the texture changes influencing L^* regard other properties than softening measured by puncture test, such as the increase in juicy texture as suggested by Penchaiya et al. (2020).

The estimated response surface plots obtained by the non-linear regression procedure well display the interplay of the time of shelf life, in this case expressed as normalized time for each color parameter, and the fruit maturity defined by δ variable, bound to μ_a540 measured at the time of pulp color measurement, and to the BSF of each individual fruit. The decrease to minimum values of L^* and h°, as well as the increase to maximum values of a^*, b^*, C^* and I_Y occurred earlier in more mature fruit (high μ_a540 value, low δ value) and later in less mature ones (low μ_a540 value, high δ value), with the same sigmoidal pattern in time.

For each color parameter, further information could be retrieved by the plot vs the specific BSF (Δt) . Considering lightness, the Δt_{L^*} values indicated that all fruit from both the transport maturities, having a negative BSF, were before the intermediate maturity in regard to L^* color parameter. In contrast, the Δt_{b^*}, Δt_{C^*}, Δt_{H° and Δt_{IY} values of fruit from both transport maturities and Δt_{a^*} values of air transport maturity fruit, having all a positive BSF, were beyond the intermediate maturity in regard to b^*, C^*, h°, I_Y and a^* color parameters. The negative Δt_{a^*} values of most of ship transport maturity fruit, on the other hand, indicated that for the ship set only few fruits were beyond the intermediate maturity in regard to a^*.

5. Conclusion

The non-destructive measurement of the absorption coefficient at 540 nm by means of TRS allowed to assess the biological age of each fruit in 'Tommy Atkins' mangoes, being μ_a540 linked to carotenoid accumulation and to pulp color changes. The μ_a540 as a function of the biological shift factor increased during ripening following a logistic/exponential model with a faster rate in less mature fruit than in more mature ones.

The changes in pulp color during mango ripening depended on fruit maturity (i.e. μ_a540) and on time of shelf life at 20 °C. By converting the μ_a540 into the biological shift factor it was possible to model the increasing trend of a^*, b^*, C^*, and I_Y and the decreasing trend of L^* and h° during the shelf life period explaining 91.2–99.8% of the variation and to differentiate mango fruit according to their biological age. Similarly to μ_a540, color changes occurred earlier in more mature fruit and later in less mature ones with the same pattern in time.

There is a synchronization between changes of μ_a540 and changes of a*, b*, C* and yellowness during ripening in mango fruit which allows to use μ_a540 to sort fruit according to their maturity degree and then to optimize fruit management along the supply chain.

Declaration of Competing Interest

The authors declare that they have no known competing financial interests or personal relationships that could have appeared to influence the work reported in this paper.

Data Availability

Data will be made available on request.

Acknowledgements

This work was funded by Lombardia Region (Italy) and Minas Gerais Region (Brazil) (Progetto di Cooperazione scientifica e tecnologica "Approccio multidisciplinare per l'innovazione della filiera di frutti tropicali – TROPICO" ID 17077, Rif. N.° AGRO-16). Thanks to Spreafico for fruit supply from commercial orchards in Pernambuco, Brazil.

Appendix A

Fig. A.1.
Fig. A.2.
Fig. B.1.

Appendix B

Table 10, Table 11, Table 12, Table 13, Table 14, Table 15.

References

Candelario-Rodríguez, H.E., Zavala-García, F., Ramírez-De León, J.A., Aranda-Ruiz, J., Montes de Oca, M.M., Velazquez, G., 2014. Effect of high pressure processing on postharvest physiology of 'Keitt' mango. Postharvest Biol. Technol. 94, 35–40. https://doi.org/10.1016/j.postharvbio.2014.03.002.

Cortés, V., Ortiz, C., Aleixos, N., Blasco, J., Cubero, S., Talens, P., 2016. A new internal quality index for mango and its prediction by external visible and near-infrared reflection spectroscopy. Postharvest Biol. Technol. 118, 148–158. https://doi.org/10.1016/j.postharvbio.2016.04.011.

Cubeddu, R., D'Andrea, C., Pifferi, A., Taroni, P., Torricelli, A., Valentini, G., Dover, C., Johnson, D., Ruiz-Altisent, M., Valero, C., 2001. Nondestructive quantification of chemical and physical properties of fruits by time-resolved reflectance spectroscopy in the wavelength range 650–1000 nm. Appl. Opt. 40, 538–543.

Dang, K.T.H., Singh, Z., Swinny, E.E., 2008. Impact of postharvest disease control methods and cold storage on volatiles, color development and fruit quality in ripe 'Kensington Pride' mangoes. J. Agric. Food Chem. 56, 10667–10674. https://doi.org/10.1021/jf801270a.

de Mello Vasconcelos, O.C., Duarte, D., de Castro Silva, J., Oliveros Mesa, F.F., Teruel Mederos, B.J., de Freitas, S.T., 2019. Modeling 'Tommy Atkins' mango cooling time based on fruit physicochemical quality. Sci. Hortic. 244, 413–420. https://doi.org/10.1016/j.scienta.2018.09.068.

De Morais, P.L.D., Filgueiras, H.A.C., De Pinho, J.L.N., Alves, R.E., 2002. Ponto decolheita ideal de mangas 'Tommy Atkins' destinadas al mercado Europeu [Harvesting maturity of mangoes 'Tommy Atkins' as for the European market]. Rev. Bras. Frutic. Jaboticabal – SP 24 (2), 671–675. https://doi.org/10.1590/S0100-29452002000300025.

Eccher Zerbini, P., Vanoli, M., Rizzolo, A., Jacob, S., Torricelli, A., Spinelli, L., Schouten, R.E., 2009. Time-resolved Reflectance Spectroscopy as a management tool in the fruit supply chain: an export trial with nectarines. Biosyst. Eng. 102, 360–363. https://doi.org/10.1016/j.biosystemseng.2008.11.002.

Eccher Zerbini, P., Vanoli, M., Rizzolo, A., Grassi, M., Pimentel, R.M.A., Spinelli, L., Torricelli, A., 2015. Optical properties, ethylene production and softening in mango fruit. Postharvest Biol. Technol. 101, 58–65. https://doi.org/10.1016/j.postharvbio.2014.11.008.

Gill, P.P.S., Jawandha, S.K., Kaur, N., 2017. Transitions in mesocarp colour of mango fruits kept under variable temperatures. J. Food Sci. Technol. 54 (13), 4251–4256. https://doi.org/10.1007/s13197-017-2894-z.

Jha, S.N., Kingsly, A.R.P., Chopra, S., 2006. Non-destructive determination of firmness and yellowness of mango during growth and storage using visual spectroscopy. Biosyst. Eng. 94, 397–402. https://doi.org/10.1016/j.biosystemseng.2006.03.009.

Kienzle, S., Sruamsiri, P., Carle, R., Sirisakulwat, S., Spreer, W., Neidhart, S., 2011. Harvest maturity specification for mango fruit (Mangifera indica L. 'Chok Anan') in regard to long supply chains. Postharvest Biol. Technol. 61, 41–55. https://doi.org/10.1016/j.postharvbio.2011.01.015.

Kienzle, S., Sruamsiri, P., Carle, R., Sirisakulwat, S., Spreer, W., Neidhart, S., 2012. Harvest maturity detection for 'Nam Dokmai #4' mango fruit (Mangifera indica L.) in consideration of long supply chains. Postharvest Biol. Technol. 72, 64–75. https://doi.org/10.1016/j.postharvbio.2012.04.011.

Lammertyn, J., Peirs, A., De Baedemaeker, J., Nicolaï, B.M., 2000. Light penetration properties of NIR radiation in fruit with respect to non-destructive quality assessment. Postharvest Biol. Technol. 18, 121–132. https://doi.org/10.1016/S0925-5214(99)00071-X.

Lu, R., Van Beers, R., Saeys, W., Li, C., Cen, H., 2020. Measurement of optical properties of fruits and vegetables: a review. Postharvest Biol. Technol. 159, 111003 https://doi.org/10.1016/j.postharvbio.2019.111003.

Martelli, F., Del Bianco, S., Ismaelli, A., Zaccanti, G., 2009. Light Propagation through Biological Tissue and Other Diffusive Media: Theory, Solutions, and Software. SPIE Press, Washington. https://doi.org/10.1117/3.824746.

Ornelas-Paz, J.J., Yahia, E.M., Gardea, A.A., 2008. Changes in external and internal color during postharvest ripening of 'Manila' and 'Ataulfo' mango fruit and relationship with carotenoid content determined by liquid chromatography-Apcl+-time-of-flight

mass spectrometry. Postharvest Biol. Technol. 50, 145–152. https://doi.org/10.1016/j.postharvbio.2008.05.001.

Padda, M.S., do Amarante, C.V.T., Garcia, R.M., Slaughter, D.C., Mitcham, E.J., 2011. Methods to analyze physico-chemical changes during mango ripening: a multivariate approach. Postharvest Biol. Technol. 62, 267–274. https://doi.org/10.1016/j.postharvbio.2011.06.002.

Penchaiya, P., Tijskens, L.M.M., Uthairatanakij, A., Srilaong, V., Tansakul, A., Kanlayanarat, S., 2015. Dynamics of Firmness and Colour of Thai Mango Cultivar 'Nam Dok Mai Si-Thong. Acta Hortic 1091, 261–266. https://doi.org/10.17660/ActaHortic.2015.1091.32.

Penchaiya, P., Tijskens, L.M.M., Uthairatanakij, A., Srilaong, V., Tansakul, A., Kanlayanarat, S., 2020. Modelling quality and maturity of 'Namdokmai Sithong' mango and their variation during storage. Postharvest Biol. Technol. 159, 111000 https://doi.org/10.1016/j.postharvbio.2019.111000.

Pereira, T., Tijskens, L.M.M., Vanoli, M., Rizzolo, A., Eccher Zerbini, P., Torricelli, A., Spinelli, L., Filgueiras, H., 2010. Assessing the harvest maturity of Brazilian mangoes. Acta Hortic 880, 269–276. https://doi.org/10.17660/ActaHortic.2010.880.31.

Rizzolo, A., Vanoli, M., 2016. Time-resolved technique for measuring optical properties and quality of food. In: Lu, R. (Ed.), Light Scattering Technology for Food Property, Quality and Safety Assessment. CRC Press, Taylor & Francis Group, Boca Raton, FL, pp. 187–224. https://doi.org/10.1201/b20220.

Rizzolo, A., Vanoli, M., Spinelli, L., Torricelli, A., 2011. Relationship between continuous wave reflectance measurement of pulp colour and the optical properties measured by time-resolved reflectance spectroscopy in various fruit species. In: Rossi, M. (Ed.), Color and Colorimetry. Multidisciplinary Contributions. Maggioli Editore, Santarcangelo di Romagna, pp. 328–335 vol. VII B.

Rizzolo, A., Vanoli, M., Spinelli, L., Torricelli, A., 2016. Non-destructive assessment of pulp colour in mangoes by time-resolved reflectance spectroscopy: problems and solutions. Acta Hortic 1119, 147–154. https://doi.org/10.17660/ActaHortic.2016.1119.20.

Rizzolo, A., Vanoli, M., Torricelli, A., Spinelli, L., Sadar, N., Zanella, A., 2021. Modeling optical properties of Braeburn apples during fruit maturation on the tree. Acta Hortic 1311, 113–121. https://doi.org/10.17660/ActaHortic.2021.1311.15.

Sabato, S.F., da Silva, J.M., da Cruz, J.N., Salmieri, S., Refa, P.R., Lacroix, M., 2009. Study of physical-chemical and sensorial properties of irradiated Tommy Atkins mangoes (Mangifera indica L.) in an international consignment. Food Control 20, 284–288. https://doi.org/10.1016/j.foodcont.2008.05.005.

Spinelli, L., Rizzolo, A., Vanoli, M., Grassi, M., Eccher Zerbini, P., Pimentel, R.M.A., Torricelli, A., 2012. Optical properties of pulp and skin in Brazilian mangoes in the 540-900 nm spectral range: implication for non-destructive maturity assessment by time-resolved reflectance spectroscopy. In: Proceedings of the 3rd CIGR International Conference of Agricultural Engineering (CIGR-AnEng2012), Valencia, Spain 8-12 July 2012. ISBN 84-615-9928-4.

Subedi, P.P., Walsh, K.B., Owens, G., 2007. Prediction of mango eating quality at harvest using short-wave near infrared spectrometry. Postharvest Biol. Technol. 43, 326–334. https://doi.org/10.1016/j.postharvbio.2006.09.012.

Tijskens, L.M.M., Heuvelink, E., Schouten, R.E., Lana, M.M., van Kooten, O., 2005. The biological shift factor. Biological age as a tool for modelling in pre- and postharvest horticulture. Acta Hortic 687, 39–46. https://doi.org/10.17660/ActaHortic.2005.687.3.

Tijskens, L.M.M., Eccher Zerbini, P., Vanoli, M., Jacob, S., Grassi, M., Cubeddu, R., Spinelli, L., Torricelli, A., 2006. Effects of maturity on chlorophyll-related absorption in nectarines, measured by non-destructive time-resolved reflectance spectroscopy. Int. J. Postharvest Technol. Innov 1 (2), 178–188. https://doi.org/10.1504/IJPTI.2006.011660.

Tijskens, L.M.M., Eccher Zerbini, P., Shouten, R.E., Vanoli, M., Jacob, S., Grassi, M., Cubeddu, R., Spinelli, L., Torricelli, A., 2007a. Assessing harvest maturity in nectarines. Postharvest Biol. Technol. 45, 204–213. https://doi.org/10.1016/j.postharvbio.2007.01.014.

Tijskens, L.M.M., Eccher Zerbini, P., Shouten, R.E., 2007b. Biological variation in ripening 0f nectarines. Vegetable Crops Research Bulletin 66, 205–212. https://doi.org/10.2478/v10032-007-0023-7.

Tijskens, L.M.M., Schouten, R.E., Konopacki, P., Jongbloed, G., Kessler, M., 2010. How to analyse non-destructive data for biological variation. In: Nunes, C. (Ed.), Environmentally Friendly and Safe Technologies for Quality of Fruits and Vegetables. Universidade do Algarve, pp. 33–40. ISBN 978-989-8472-01-4.

Torricelli, A., Spinelli, L., Contini, D., Vanoli, M., Rizzolo, A., Eccher Zerbini, P., 2008. Time-resolved reflectance spectroscopy for nondestructive assessment of food quality. Sens. Instrum. Food Qual. Saf. 2, 82–89. https://doi.org/10.1007/s11694-008-9036-2.

Vásquez-Caicedo, A.L., Heller, A., Neidhart, S., Carle, R., 2006. Chromoplast morphology and β-carotene accumulation during postharvest ripening of Mango cv. 'Tommy Atkins. J. Agric. Food Chem. 54, 5769–5776. https://doi.org/10.1021/jf060747u.

Vanoli, M., Pereira, T., Grassi, M., Spinelli, L., Filgueiras, H., Tijskens, L.M.M., Rizzolo, A., Torricelli, A., 2011. Changes in pulp colour during postharvest ripening of 'Tommy Atkins' mangoes and relationship with optical properties measured by time-resolved reflectance spectroscopy. In: CD-ROM Proceedings 6th CIGR Section VI International l Symposium "Towards a sustainable food chain: Food Process, Bioprocessing and Food Quality Management" April 18-20, 2011, Nantes, France (4 pages) ISBN 978-2-7466-3203-5.

Vanoli, M., Rizzolo, A., Grassi, M., Spinelli, L., Eccher Zerbini, P., Pimentel, R.M.A., Torricelli, A., 2013. Quality of Brazilian mango fruit in relation to optical properties non-destructively measured by time-resolved reflectance spectroscopy. In: Bellon Maurel, V., Williams, P., Downey, G. (Eds.), NIR 2013 Proceedings– Picking up good vibrations. Montpellier. IRSTEA, pp. 177–181.

Vanoli, M., Rizzolo, A., Spinelli, L., Azzollini, S., Torricelli, A., 2016. Carotenoid content and pulp colour non-destructively measured by time-resolved reflectance spectroscopy in different cultivars of Brazilian mangoes. Acta Hortic 1119, 305–312. https://doi.org/10.17660/ActaHortic.2016.1119.42.

Vanoli, M., Grassi, M., Spinelli, L., Torricelli, A., Rizzolo, A., 2018. Quality and nutraceutical properties of mango fruit: influence of cultivar and biological age assessed by Time-resolved Reflectance Spectroscopy. Adv. Hort. Sci. 32, 407–420. https://www.jstor.org/stable/26613270.